Cancer Chemother Pharmacol (2009) 64:811–827
DOI 10.1007/s00280-009-0932-x

ORIGINAL ARTICLE

Doxorubicin-induced mitochondrial dysfunction is secondary to nuclear p53 activation in H9c2 cardiomyoblasts

Vilma A. Sardão · Paulo J. Oliveira · Jon Holy · Catarina R. Oliveira · Kendall B. Wallace

Received: 14 August 2008 / Accepted: 9 January 2009 / Published online: 30 January 2009

Abstract
Purpose Doxorubicin (DOX) is a widely prescribed chemotherapeutic. The hypothesis for the present study is that DOX-induced myocyte apoptosis involves mitochondrial dysfunction that is a consequence of nuclear DOX effects.
Methods H9c2 myoblasts were incubated with 0, 0.5 and 1 μM DOX and nuclear and mitochondrial alterations were determined.
Results Doxorubicin accumulation in the nucleus was detected after 3 h treatment, followed by an increase in p53 and a decrease in mitochondrial membrane potential. Apoptotic markers, such as caspase activation and chromatin condensation were detected after 24 h of DOX treatment. Bax and p53 translocation to mitochondria as well as the formation of Bax clusters in the cytosol were observed. Importantly, pifithrin-alpha, a p53 inhibitor, protected against DOX-induced mitochondrial depolarization, caspase activation and cell death.
Conclusion Mitochondrial dysfunction in H9c2 myoblasts treated with DOX is a consequence of nuclear p53 activation rather than a direct effect of the drug on mitochondria.

Keywords H9c2 myoblast · Doxorubicin · p53 · Bax · Cardiomyopathy · Oxidative stress

V. A. Sardão (✉) · P. J. Oliveira
Department of Zoology,
Center for Neurosciences and Cellular Biology,
University of Coimbra, 3004-517 Coimbra, Portugal
e-mail: vimarisa@ci.uc.pt

J. Holy
Department of Anatomy, Microbiology and Pathology,
University of Minnesota Medical School, Duluth, USA

C. R. Oliveira
Department of Biochemistry,
Center for Neurosciences and Cellular Biology,
Medical School, University of Coimbra, Coimbra, Portugal

K. B. Wallace
Department of Biochemistry and Molecular Biology,
University of Minnesota Medical School, Duluth, USA

Introduction

Doxorubicin (Adriamycin©, DOX), an anthracycline analog, is one of the most frequently prescribed anti-neoplastic agents for cancer chemotherapy. However, the dose-dependent cardiotoxicity induced by DOX, which eventually results in refractory cardiac dysfunction, compromises its clinical application. The pro-oxidant action of DOX on cardiac cells has been implicated as the major mechanism responsible for the cardiotoxicity [1]. The chemical properties of DOX support redox cycling on complex I of the mitochondrial respiratory chain [2] and the generation of reactive oxygen species (ROS), such as H_2O_2 and superoxide anion [3]. Damage to cardiac mitochondria includes specific and non-specific membrane interactions [4], lipid peroxidation in mitochondrial membranes [5], preferential oxidation of mitochondrial DNA [6] and the activation of the calcium-dependent, cyclosporin-A-sensitive permeability transition pore (MPTP) [7]. The redox-sensitive MPTP has been implicated in cardiomyocyte dysfunction and cell death [8, 9] and may be a determinant in cellular fate following myocardial ischemia and reperfusion [10].

In view of its pro-oxidant properties DOX may induce cell death through oxidative damage to mitochondria. The involvement of mitochondria in the induction of apoptosis by DOX in cardiac cells has already been demonstrated [11, 12].

It has been reported that the anti-neoplastic activity involves DOX interfering with DNA stability and compromising cell integrity [13, 14]. However, the relevance of DOX interaction with nuclear DNA of cardiac cells is only now beginning to be understood. In this context, it has been reported that DNA damage and signaling pathways involving the tumor suppressor p53 and mitochondria are early events in DOX-induced cardiac cell death [15]. Furthermore, pifithrin-alpha, a cell-permeant p53 inhibitor, protects against DOX-induced apoptosis in cardiac cells [16, 17]. In vivo studies have also shown that disruption of the p53 gene reduces DOX-induced cardiotoxicity and attenuates the decline of left ventricle systolic function, apoptosis of cardiac myocytes, and the depletion of myocardial glutathione and Cu/Zn superoxide dismutase [18]. Therefore, p53-mediated signals play a significant role in DOX-induced cardiac toxicity and may modulate DOX-induced oxidative stress.

More than just being a 'guardian of the genome', p53 can also act directly as a pro-apoptotic protein, being translocated to mitochondria and activating the mitochondrial-dependent (intrinsic) pathway of apoptosis, which occurs independently of new gene transcription or protein synthesis [19–21]. Recent studies provide insight into the role of p53 as a bridge between the nucleus and mitochondria in cardiac cells upon DOX treatment [22, 23].

The present work was directed at testing the hypothesis that mitochondrial dysfunction occurs secondarily to p53 nuclear activation and involves the pro-apoptotic protein Bax. By testing the work hypothesis and by learning more about the temporal and spatial interaction of DOX with cardiac cells, new targets involved in DOX cardiotoxicity can be revealed and the rational design of new treatment strategies can be made to minimize cardiomyopathies associated with DOX chemotherapy.

Materials and methods

Reagents

Dulbecco's modified Eagle's medium (DMEM), penicillin, streptomycin, fetal bovine serum and Trypsin–EDTA were purchased from Gibco-Invitrogen (Grand Island, NY). DOX, *N*-acetylcysteine (NAC), vitamin E-succinate, cyclosporin A, sulforhodamine B (SRB), 5-bromo-2′-deoxyuridine (BrdU), DL-dithiothreitol (DTT), phenylmethanesulfonyl fluoride (PMSF) and protease inhibitor cocktail were obtained from Sigma (St Louis, MO). Pifithrin-alpha and caspase substrates were purchased from Calbiochem (San Diego, CA). Hoechst 33342, tetramethylrhodamine methyl ester (TMRM), Mitotracker Red CMXROS and 5-(and-6)-chloromethyl-2′, 7′-dichlorodihydrofluorescein diacetate (CM-H_2DCFDA) were obtained from Molecular Probes (Eugene, OR). Mouse monoclonal anti-BAX antibody for immunocytochemistry and mouse monoclonal anti-cytochrome *c* antibody were purchased from BD Bioscience Pharmingen (San Diego, CA). Goat polyclonal anti-p53 antibody was purchased from Santa Cruz (Santa Cruz, CA). Rabbit polyclonal anti-Bax antibody for Western blot was purchased from Cell Signaling (Danvers, MA). Mouse monoclonal Anti-BrdU antibody (G3G4) was purchased from Developmental Studies Hybridoma Bank (Iowa City, IA). All secondary antibodies fluorescein (FITC) and alkaline phosphatase (AP)-conjugated were purchased from Jackson ImmunoResearch Laboratories, Inc. (Cambridgeshire, UK).

Cell culture and treatments

The H9c2 cell line, originally derived from embryonic rat heart tissue using selective serial passages [24], was purchased from America Tissue Type Collection (Manassas, VA; catalog #CRL-1446). The myoblastic cell line H9c2 [24] has been used as an in vitro model for cardiac muscle for the study of mechanisms involved in DOX-induced cardiotoxicity [25].

Cells were cultured in DMEM medium supplemented with 1.5 g/l sodium bicarbonate, 10% fetal bovine serum, 100 U/ml of penicillin and 100 μg/ml of streptomycin in 75 cm^2 tissue culture flasks at 37°C in a humidified atmosphere of 5% CO_2. Cells were fed every 2–3 days, and sub-cultured once they reached 70–80% confluence. For mitochondrial $\Delta\psi$ evaluation, calcium deregulation and oxidative stress, cells were seeded at a density of 35,000 cells per ml in glass-bottom dishes (Mat-Tek Corporation, Ashland, MA). For SRB assays, cells were seeded as described above but in 24-well plates (final volume of 1 ml/well). For detection of chromatin condensation studies and immunocytochemistry assays cells were seeded in six-well plates containing glass coverslips (final volume of 2 ml/well at a density of 35,000 cells per ml). For Western blot analysis and caspase 3 and 9-like activity measurement, cells were seeded in 75 cm^2 tissue culture flasks at a sub-cultivation ratio of 1:5. The cells were then allowed to grow for 4–5 days in order to reach the desired confluence (~80–90%). The cells were seeded in DMEM with 10% FBS and experiments were carried out up to 24-h post-treatment. DOX was directly added to the cell culture media at described concentrations. In experiments involving Pifithrin-alpha and trolox, cells were pre-incubated with the respective compound concentration for 30 min at 37°C before DOX treatment. In experiments involving vitamin E-succinate, cells were pre-incubated with the respective concentration of compound for 24 h before treatment with DOX. In experiments involving NAC, cells were pre-incubated with respective compound concentration for 2 h at 37°C before

DOX treatment. All compounds were maintained in the media until the end of the experiment. In experiments involving cyclosporin A, cells were pre-incubated with the compound (1 μM) for 15 min at 37°C before DOX treatment. The concentration of inhibitors and antioxidants used was the maximum concentration that did not cause cell death by itself. Controls with vehicle (ethanol or DMSO) were also performed the in same conditions. In the present study, DOX concentrations of 0.5 and 1 μM were used due to their clinical relevance, as the concentrations fall well within the concentrations of DOX found in the plasma of patients undergoing DOX therapy [26].

Detection of DNA synthesis by BrdU labeling

The H9c2 cells were seeded on glass coverslips in six-well plates and incubated with or without 0.5 and 1 μM DOX during 6, 12 and 24 h. Afterwards, cells were pulse-labeled with 10 μM BrdU for 30 min at 37°C, rinsed with PBS, fixed and stored at −20°C in ice-cold absolute methanol until use. For BrdU labeling, cells were rehydrated with PBST (PBS supplemented with 0.05% Tween-20) and treated with 2 N HCl for 20 min at room temperature in order to denaturate DNA. The cells were than rinsed five times with PBST and incubated in blocking solution (PBST supplemented with 1% non-fat powdered milk) for 30 min at 37°C. Anti-BrdU antibody (dilution 1:50) was added for 2 h at 37°C. After three washes of 5 min each with PBST the cells were incubated with goat anti-mouse antibody conjugated to FITC (dilution 1:50), containing also 5 μg/ml Hoechst 33258 for 2 h at 37°C. The coverslips were finally washed in PBST and mounted in anti-fade medium consisting of nine parts glycerol and one part 0.1 M CAPS buffer, pH 9.0, supplemented with 0.1% phenylenediamine and 0.1% DABCO (both from Sigma Chemical Co.). The cells were observed by epifluorescence microscopy using a Nikon Eclipse TE2000U microscope equipped with 40× Plan Fluor 0.6 NA phase contrast objective. Images were processed using Metamorph software (Universal Imaging, Downingtoen, PA).

Immunofluorescence and confocal microscopy

For Bax immunolabeling, cells were incubated with Mitotraker red (125 nM) for 30 min at 37°C in the dark, washed with cold PBS and fixed with 4% paraformaldehyde during 15 min at room temperature. The cells were rinsed with PBS and stored in PBST at 4°C until use. For p53 immunolabeling, cells were fixed and stored at −20°C in ice-cold absolute methanol. The cells fixed with paraformaldehyde were permeabilized with 0.2% Triton X-100 in PBS for 5 min at room temperature, following three washes with PBS. The cells fixed with ice-cold methanol were not permeabilized, but rehydratated with PBST for 5 min thrice. Later the cells were incubated in blocking solution (PBST supplemented with 1% non-fat powdered milk) for 30 min at 37°C, probed with specific primary antibody (p53, 1:50; Bax, 1:20) for 2 h at 37°C and stained with FITC-conjugated secondary antibodies (rabbit anti-goat for p53 and goat anti-mouse for Bax, dilution 1:50), containing 5 μg/ml of Hoechst 33342, for an additional 2 h at 37°C. Between labeling with primary and secondary antibodies, cells were rinsed with PBST three times for 5 min each. The coverslips were mounted on glass slides in an anti-fade medium as described previously. The cells were observed by epifluorescence microscopy using a Nikon Eclipse TE2000U microscope. The fluorescein filter was used for FITC imaging and the rhodamine filter for Mitotracker red and TexRed fluorescence imaging. The Hoechst signal was obtained using the UV filter. Images were obtained using Metamorph software (Universal Imaging, Downington, PA). For p53 analysis, cells were observed by epifluorescence microscopy using a Nikon Eclipse TE2000U microscope equipped with 40× Plan Fluor 1.3 NA oil immersion DIC objective and images were processed using Metamorph software (Universal Imaging, Downingtoen, PA). Images showing Bax clusters were taken using a Nikon C-1 laser scanning confocal microscope equipped with 60× Plan Apo 1.4 NA oil immersion DIC objective. Images were captured using the Nikon EZ-C1 software (version 2.01). The number of cells showing Bax clusters was counted and expressed as the percentage of total cells analyzed.

Collection of total and mitochondrial extracts from H9c2 cells

To obtain total cellular extracts H9c2 cells were harvested by trypsinization and washed once with PBS, after treatment with DOX. Floating cells were also collected and combined with adherent cells. In order to collect total cells, two centrifugation steps were performed for 5 min at 1,000×*g*. Cellular pellet was resuspended in collecting buffer (20 mM HEPES/NaOH, pH 7.5, 250 mM Sucrose, 10 mM KCl, 2 mM $MgCl_2$, 1 mM EDTA) supplemented with 2 mM DTT, 100 μM phenylmethylsulfonyl fluoride (PMSF) and a protease inhibitor cocktail (containing 1 μg/ml of leupeptin, antipain, chymostatin and pepstatin A) and ruptured by 30 passages through a 27-gauge needle. The cell suspension was then rapidly frozen/thawed thrice in liquid nitrogen and kept at −80°C until used. For subcellular fractionation, cells were harvested as described above and resuspended in homogenization buffer (250 mM sucrose, 20 mM K^+ Hepes pH 7.5, 10 mM KCl, 1.5 mM $MgCl_2$, 0.1 mM EDTA, 1 mM EGTA) supplemented with 1 mM DTT, 100 μM PMSF and protease inhibitor cocktail (containing 1 μg/ml of leupeptin, antipain, chymostatin and

pepstatin A). Cell homogenization was performed in a Potter–Elvehjem homogenizer with a Teflon pestle. The homogenate was subjected to sedimentation at 220×*g* for 5 min at 4°C. The supernatant, containing mitochondrial fraction, was centrifuged again at 14,000×*g* for 10 min at 4°C. The pellet, corresponding to the mitochondrial fraction was resuspended in 50 µl of homogenization buffer and the supernatant was again centrifuged at 100,000×*g* for 30 min at 4°C. In order to concentrate protein, supernatant, containing the cytosolic fraction was lyophilized, and resuspended in 50 µl of water. Samples were stored at −80°C until used. Protein contents were determined by the Bradford method.

Western blotting analysis

After denaturation at 100°C for 5 min in a *Laemmli* buffer (from Bio-Rad) an equivalent amount of proteins (50 µg) was separated by electrophoresis on 8 or 12% SDS–polyacrylamide gels (SDS–PAGE) and electrophoretically transferred to a polyvinylidene difluoride (PVDF) membrane. After blocking with 5% milk in TBST (50 mM Tris–HCl, pH 8; 154 mM NaCl and 0.1% tween 20) for 2 h at room temperature, membranes were incubated overnight at 4°C with the antibodies directed against the denaturated form of p53 (goat anti-p53; 1:200), Bax (rabbit anti-Bax; 1:8,000) and cytochrome *c* (mouse anti-cytochrome *c*; 1:1,000). The membranes were further incubated with secondary antibodies rabbit anti-goat IgG (for anti-p53 antibody; 1:5,000), goat anti-rabbit IgG (for anti-Bax antibody; 1:2,500) or rabbit anti-mouse (for anti-cytochrome *c* antibody; 1:2,500), AP-conjugated, for 2 h at room temperature. The membranes were incubated with the ECF detection system (from Amersham) and read with the Versa Doc imaging system (Bio-Rad). The densities of each band were calculated with Quantity One Software (Bio-Rad) and expressed as a percentage of control. The membranes were stained with Ponceau reagent as protein loading control in each lane, a method that has been considered efficient and accurate to confirm equal protein load [27].

Caspase-like activity assay

Total cellular extracts were collected as described above and protein contents were assayed using the Bradford method. To measure caspase 3 and 9-like activity, aliquots of cell extracts containing 25 µg (for caspase 3) or 50 µg (for caspase 9) were incubated in a reaction buffer containing 25 mM Hepes (pH 7.4), 10% sucrose; 10 mM DTT, 0.1% CHAPS and 100 µM caspase substrate (Ac-DEVD-*p*NA for caspase 3 or Ac-LEHD-*p*NA for caspase 9, purchased from Calbiochem) for 2 h at 37°C. Caspase-like activities were determined by following the detection of the chromophore *p*-nitroanilide after cleavage from the labeled substrate Ac-DEVD-*p*-nitroanilide or Ac-LEHD-*p*-nitroanilide. The method was calibrated with known concentrations of *p*-nitroanilide (purchased from Calbiochem).

Chromatin condensation detection

The nuclear morphology of cells was studied by using the cell-permeable DNA dye Hoechst 33342. After DOX treatment, cells were washed twice with PBS, fixed with 2 ml of ice cold absolute methanol and stained with 1 µg/ml of Hoechst 33342 for 30 min at 37°C in the dark. Nuclear morphological changes were detected by using an epifluorescence Nikon Eclipse TE2000U microscope (UV filter) equipped with 40× Plan Fluor 0.6 NA phase contrast objective. Images were processed using Metamorph software (Universal Imaging, Downingtoen, PA). Two hundred cells from several randomly chosen fields were counted and the number of apoptotic cells was expressed as percentage of the total number of cells counted.

Cytotoxicity and cell density evaluation by sulforhodamine B assay

Sulforhodamine B assays were conducted in order to evaluate the cytotoxic effects of DOX and the protective effect of pifitrhin-alpha, trolox, vitamin E-succinate and NAC. Following treatment, the incubation media were removed and cells were fixed in 1% acetic acid in ice-cold methanol for at least 30 min. The cells were then incubated with 0.5% (wt/vol) SRB dissolved in 1% acetic acid for 1 h at 37°C. Unbound dye was emoved with 1% acetic acid. Dye bound to cell proteins was extracted with 10 mM Tris base solution, pH 10, and the optical density of the solution was determined at 540 nm. The results were expressed as a percentage of control.

Detection of intracellular oxidative stress with 5-(and-6)-chloromethyl-2′, 7′-dichlorodihydrofluorescein diacetate

After DOX treatment, H9c2 cells in glass-bottom dishes were incubated with the probe CM-H_2DCFDA (7.5 µM) for 1 h at 37°C in the dark. The culture media was then replaced by new pre-warmed DMEM and then cells were returned to the incubator for another hour. The media was again replaced by 2 ml of Krebs buffer (1 mM $CaCl_2$; 132 mM NaCl; 4 mM KCl; 1.2 mM Na_2HPO_4; 1.4 mM $MgCl_2$; 6 mM Glucose; 10 mM HEPES, pH 7.4). The cells were observed by epifluorescence microscopy using a Nikon Eclipse TE2000U microscope (fluorescein filter) equipped with 40× Plan Fluor 1.3 NA oil immersion DIC objective and images were obtained using Metamorph

software (Universal Imaging, Downingtoen, PA). The results were expressed as a function of control dishes.

Alterations of mitochondrial membrane potential induced by DOX

Alteration in mitochondrial membrane potential was evaluated using the probe TMRM, in a non-quenching mode. After DOX treatment, H9c2 cells cultured in glass-bottom dishes were incubated with the probe TMRM (100 nM) for 30 min at 37°C in the dark. Due to the very low fluorescence of the probe in the extracellular media, the images were collected without replacing the cell culture media. The cells were observed by epifluorescence microscopy using a Nikon Eclipse TE2000U microscope. The results were expressed as a function of control dishes.

Measurement of the intracellular calcium levels

Alteration in intracellular calcium levels was evaluated using the ratiometric probe FURA-2/AM. After DOX treatment, media was replaced by 2 ml of Krebs buffer (1 mM $CaCl_2$; 132 mM NaCl; 4 mM KCl; 1.2 mM Na_2HPO_4; 1.4 mM $MgCl_2$; 6 mM Glucose; 10 mM HEPES, pH 7.4), supplemented with 1 mg/ml bovine serum albumin (BSA) and 5 μM FURA-2/AM, and incubated at 37°C for 40 min. Afterwards, the Krebs buffer containing the probe was removed and cells were rinsed with PBS and incubated in fresh Krebs buffer supplemented with BSA but without probe. The cells were observed by epifluorescence microscopy using an Axiovert 200 epifluorescence inverted microscope (Zeiss) equipped with PAN-Neofluar 40×, 1.30 NA oil immersion and phase ph3 objective. Images were obtained using MetaFluor software (Universal Imaging Corporation, ver. 5.0r7 2003). Individual fluorescence of each cell was ratiometrically measured with excitation wavelength at 340 and 380 nm and emission wavelength at 510 nm. The results were expressed as a function of control dishes. Calibration with ionomycin/EGTA was not performed due to sudden changes in cell morphology which interfere with probe fluorescence (data not shown). When EGTA was added, H9c2 cells immediately rounded up and the fluorescence signal was altered, not because of calcium alterations but due to changes in cell morphology and volume (data not shown).

Statistical analysis

Data are expressed as mean ± SEM for the number of experiments indicated in the legends of the figures. Multiple comparisons were performed using one-way analysis of variance (ANOVA) followed by a Bonferroni post hoc test. Significance was accepted with $P < 0.05$.

Results

Nuclear accumulation of Doxorubicin

A temporal evaluation of DOX nuclear accumulation in H9c2 cells was initially performed. As DOX is a fluorescent molecule, its accumulation and intracellular distribution in H9c2 cells can be detected by epifluorescence microscopy. At pre-determined time points (0, 30, 45, 60, 90, 120, 180 and 240 min after addition), images were collected using identical exposure and camera settings, and the fluorescence of selected regions of interest was subsequently measured. As demonstrated in Fig. 1a, an increase in nuclear fluorescence was detected over time upon cell treatment with 1 μM DOX. Simultaneously, an increase in background fluorescence was also observed, which can be attributed to a slight pH increase of the media. For this reason, the increase in nuclear fluorescence was calculated as the ratio of nuclear to background fluorescence intensity for each time point studied (Fig. 1b). DOX nuclear uptake displays sigmoid kinetics, reaching a plateau 180 min (3 h) after DOX addition. An exponential increase in nuclear DOX fluorescence was observed between 30 and 120 min (2 h) after DOX addition. Besides real-time measurements of DOX nuclear accumulation, we also incubated DOX with separate sets of cells which were kept in the incubator and observed at some of the selected time points, thus excluding artifacts due to repeated examination of the same sample over time (e.g., photobleaching). The results obtained were very similar (data not shown). The H9c2 cells treated with DOX vehicle (water) did not show an increase in nuclear fluorescence, suggesting that the nuclear fluorescence observed in the treated group was resulting from DOX accumulation (data not shown). Nuclear DOX fluorescence was also co-localized with Hoechst 33343 nuclear fluorescence; in fact, Hoechst nuclear fluorescence was decreased in the presence of DOX, confirming a spatial interaction between both molecules (data not shown). Nevertheless, at this point we cannot exclude that DOX can also be accumulated by other organelles besides the nucleus, although the fluorescence was not easily detected using the present method.

Effects of Doxorubicin on DNA synthesis during cell proliferation

The effect of DOX on DNA synthesis was analyzed by using the bromodeoxyuridine (BrdU) labeling assay. The H9c2 cells were treated with DOX for 2, 6, 12 and 24 h and then pulse-labeled with 10 μM of BrdU for 30 min. A slight but insignificant reduction in BrdU incorporation was observed at 2, 6 and 12 h of DOX treatment. A significant

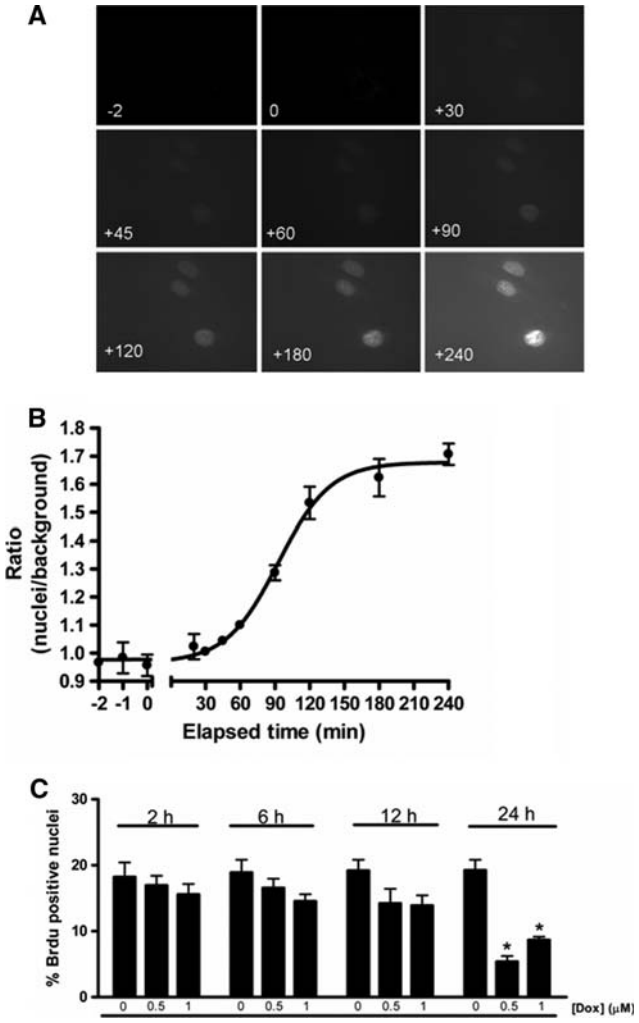

Fig. 1 Doxorubicin nuclear uptake and effects on DNA synthesis in H9c2 cells. **a** Epifluorescence microscopy images of H9c2 cells treated with 1 μM DOX. At the described time points (in min), the images were collected in the rhodamine channel, which resulted in a nuclear signal due to DOX self-fluorescence and nuclear accumulation. **b** Ratio between nuclear and background fluorescence of selected regions of interest for each time point. The *graph* represents the kinetic of DOX accumulation in H9c2 nuclei. *Error bar* represent SEM obtained from four different experiments. **c** After DOX treatment and before fixation, H9c2 cells were pulsed with 10 μM BrdU for 30 min at 37°C. Cells were then labeled with an antibody against BrdU and counterstained with Hoechst 33342. The numbers of BrdU positive nuclei were counted and expressed as the percentage of total nuclei counted. Approximately 200 nuclei were counted per coverslip. Data represents the mean and SEM of five different experiments. * $P < 0.05$ versus absence of DOX treatment for the respective time point

inhibition of BrdU incorporation was only evident after 24 h of DOX treatment (Fig. 1c).

Doxorubicin treatment promotes an increase in p53 and Bax proteins

Alterations in p53 concentration induced by DOX treatment were analyzed by both immunocytochemistry and Western blot assays (Fig. 2a, b). For immunocytochemistry experiments (Fig. 2a), control and treated cells were fixed and labeled with an antibody against p53. The results demonstrate that when incubated with cells for 24 h, DOX (both 0.5 and 1 μM) promotes an increase in p53 nuclear fluorescence intensity. For Western blots, H9c2 cells were treated with 0.5 and 1 μM DOX for 6, 12 and 24 h (Fig. 2b) and total cell extracts were analyzed. The data obtained show an increase of p53 protein content occurred as early as 6 h of treatment. An increase in Bax concentration was also detected by Western blot in whole cell extracts from H9c2 myoblasts after treatment with 0.5 and 1 μM DOX for 24 h (Fig. 2c). The cells treated with DOX vehicle showed no p53 increase with time.

Doxorubicin promotes translocation of p53 and Bax to mitochondria and formation of Bax clusters

The presence of Bax and p53 in mitochondrial fraction after H9c2 treatment with DOX was analyzed by Western blot (Fig. 3a). COX IV was used to confirm equivalent mitochondrial enrichment in each fraction (data not shown). Possible contamination with nuclear fraction was checked by using the antibody H2AX which reacts against nuclear histones (data not shown). Equal protein loading was confirmed by Ponceau staining. The results demonstrate an increase in the quantity of p53 and Bax in mitochondrial fractions isolated from H9c2 cells treated with 1 μM of DOX for 24 h. Treatment with 0.5 μM DOX also promotes an increase in the amount of Bax in the mitochondrial fraction. However, the same result was not observed for p53. Alterations in Bax localization were also analyzed by confocal microscopy (Fig. 3b, c). According to the results obtained by confocal microscopy (Fig. 3b), the formation of Bax clusters (or foci) was observed after 24 h treatment with 0.5 and 1 μM DOX. In contrast, Bax immunolabeling was low and homogeneously distributed throughout control cells.

It is interesting to note that by examining in detail some of the cells exhibiting Bax clusters, such regions of intense Bax immunoreactivity are located on or very close to polarized mitochondrial filaments (Fig. 3c). In the particular example shown in Fig. 3c (upper row), Bax clusters and polarized mitochondria (i.e., with Mitotracker fluorescence) appear to form a continuous filament, suggesting that the formation of Bax clusters were part of the fragmentation process of an otherwise long mitochondrial filament. Longitudinal views of H9c2 myoblasts confirmed that Bax clusters are present within and not above or under the cell body. As shown in the graph of Fig. 3c, treatment with 0.5 μM DOX for 24 h promotes an increase in the number of H9c2 cells showing Bax foci. No significant formation of Bax foci was observed by epifluorescence and confocal microscopy after 6 and 12 h of DOX treatment (data not shown).

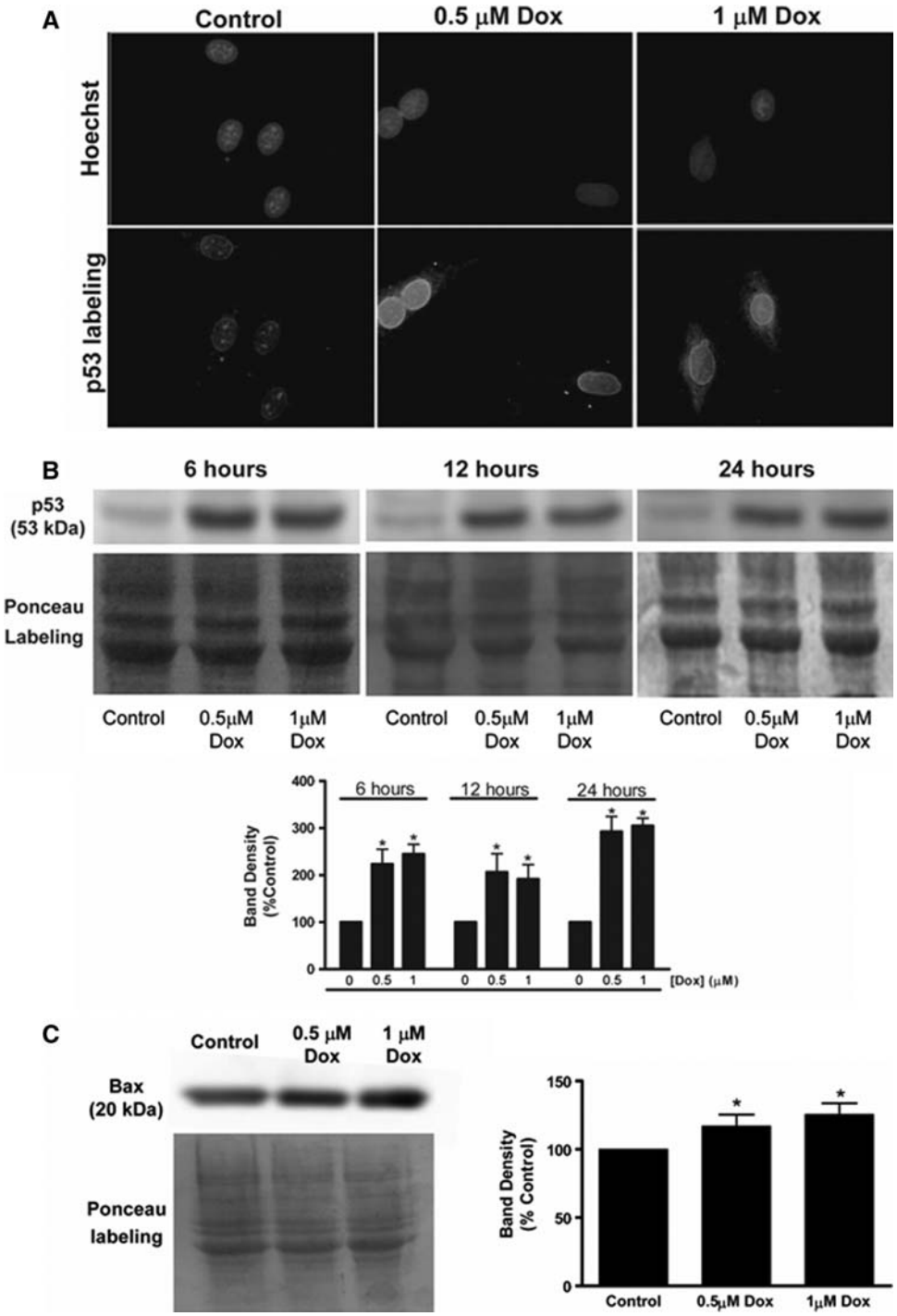

Fig. 2 Doxorubicin treatment increases p53 and Bax concentration in H9c2 myoblasts. **a** Epifluorescence microscopy images of nuclei showing H9c2 cells treated with 0, 0.5 and 1 μM DOX over 24 h. After treatment, cells were fixed, labeled with an antibody against p53 and counterstained with Hoechst 33342. Epifluorescence microscopy images illustrate increased p53 nuclear labeling after H9c2 cells treatment with DOX. **b** p53 concentration in total cellular extracts, identified by Western blot analysis as a protein band of 53-kDa. Total cellular extracts were collected after treating H9c2 cells with 0, 0.5 and 1 μM DOX for 6, 12 and 24 h, as described in "Materials and methods" section. Images are representative experiments from four separate assays producing similar results. *Ponceau labeling* shows the loading of equal amount of protein in each line. *Plot* represents densitometric analysis of p53 protein, expressed as % of control. Data are expressed as mean ± SEM of four different experiments. Statistical analysis * $P < 0.05$ compared with control for the respective time point. **c** Bax contents in total cellular extracts, identified by Western blot as a band of 21-kDa. Total cellular extracts were collected after H9c2 cells treatment with 0, 0.5 and 1 μM DOX during 24 h. Images are representative experiments from four different assays producing similar results. *Ponceau labeling* shows the loading of equal amount of protein in each lane. *Plot* represents densitometric analysis of Bax protein, expressed as % of control. Data are expressed as mean ± SEM of four different experiments. Statistical analysis * $P < 0.05$ compared with control

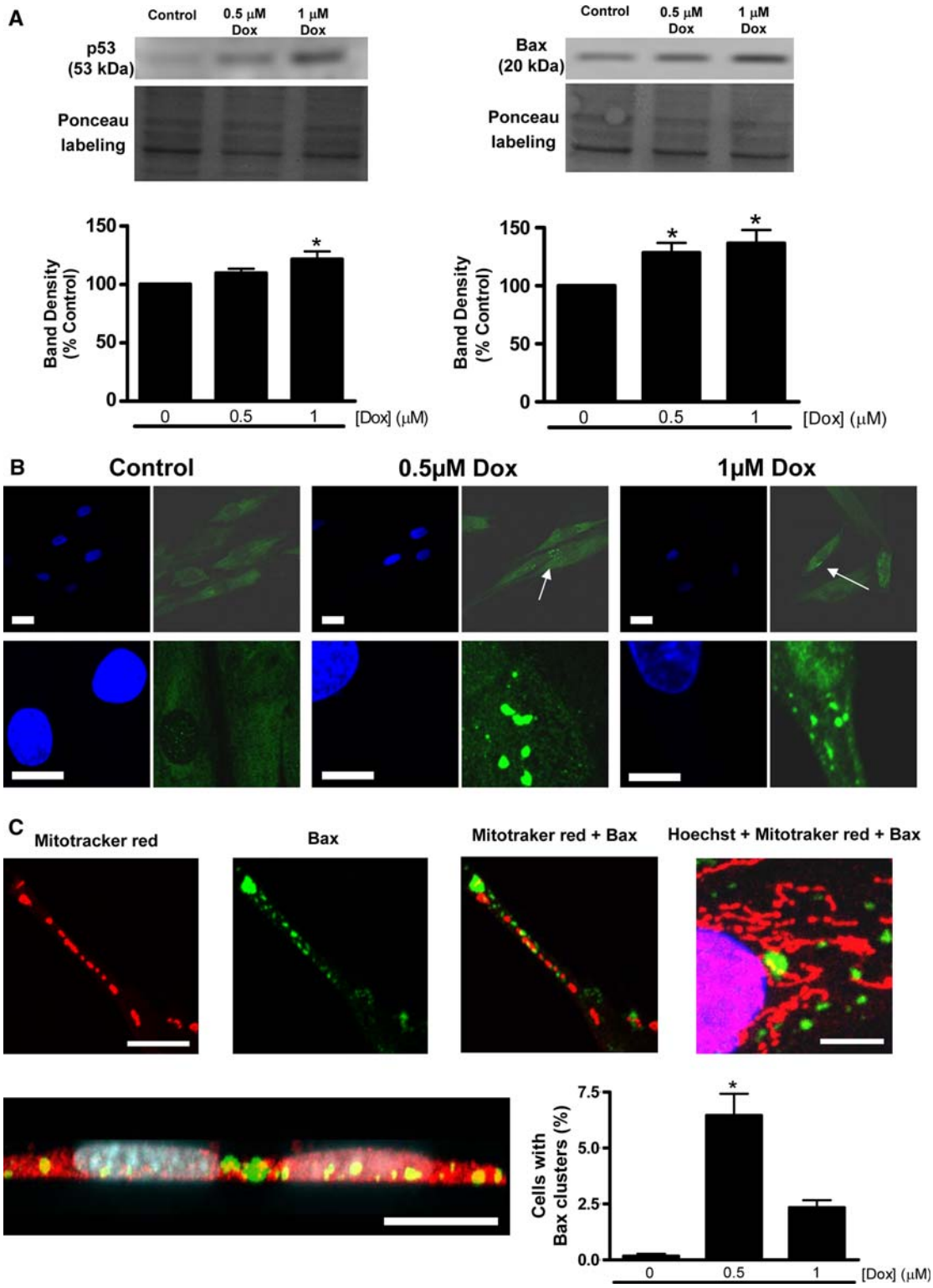

Doxorubicin induces cytochrome *c* release from mitochondria and activation of caspase 9 and caspase 3

After DOX treatment, cytochrome *c* release from mitochondria to cytosol was analyzed by Western blot (Fig. 4a). An increase of cytochrome *c* in the cytosolic fraction after treatment of H9c2 cells with 1 μM DOX for 24 h was observed, which was in agreement with a decrease in the same protein present in the mitochondrial fraction (Fig. 4a). However, cytochrome *c* release was not apparent after treatment with 0.5 μM during the same time period.

◀ **Fig. 3** DOX induces p53 and Bax translocation to mitochondria and the formation of cytosolic Bax clusters. **a** Western blot analysis of mitochondrial fractions collected from H9c2 cells after 24 h treatment with 0, 0.5 and 1 μM DOX. Mitochondrial fraction was collected as described in "Materials and methods" section. Western blot images are representative from six different experiments, producing similar results. *Ponceau labeling* shows the loading of equal amount of protein in each line. *Graphs* represent the densitometric analysis of p53 and Bax protein in mitochondrial fraction, expressed as % of control. Data are expressed as mean ± SEM of six different experiments. **b** Confocal microscopy of H9c2 cells treated with 0, 0.5 and 1 μM DOX for 24 h. After treatment, cells were fixed in paraformaldehyde and subsequently labeled with an antibody against Bax (*green*). Two rows of images of different magnifications are shown (*bar* corresponds to 20 mm). The formation of Bax clusters is visible in the images with higher magnification. The *arrows* indicate the Bax clusters. **c** *Upper panel* laser scanning confocal microscopy images of mitochondrial filaments from H9c2 cells treated with 0.5 μM DOX for 24 h. *Images* show the labeling with Mitotracker red (*red*), Bax (*green*), and Hoechst 33342 (*blue–pink*). *Panels* are the same magnification. *Scale bar* corresponds to 10 μm. *Lower panel* longitudinal view of two H9c2 cells treated with DOX, obtained by performing a 3-D Z-stack with a confocal microscopy. The image confirms that Bax clusters are located in the same focal plane as other cell structures and not above or below the cell body. *Bar* corresponds to 20 μm. The number of cells showing Bax clusters were counted and expressed as the percentage of total cells analyzed. Data are expressed as mean ± SEM of four different cell preparations. Statistical analysis * $P < 0.05$ compared with control

Doxorubicin-induced increase in caspase-9 (Fig. 4b) and caspase-3-like activities (Fig. 4c) were also analyzed in H9c2 cells. The results show increased caspase-9-like activity after treatment with 1 μM DOX for 12 (data not shown) and 24 h (Fig. 4b). Although an increase in the activity of caspase-9 was also detected after treatment with 0.5 μM, the result was not statistically significant. On the other hand, an increase of caspase-3-like activity for both 0.5 and 1 μM DOX after 12 (data not shown) and 24 h (Fig. 4c) incubation was observed.

Apoptotic nuclear alterations induced by Doxorubicin

Nuclear morphologic changes typical of apoptosis were detected by imaging nuclei stained with Hoechst 33342 after DOX treatment (Fig. 4d, upper panel). At time zero (no DOX added), only 1.5 ± 0.6% of cells showed condensed chromatin. However, by incubating DOX for 24 h, the number of H9c2 cells displaying condensed chromatin increased to 16.5 ± 5.7% after treatment with 0.5 μM and to 13.2 ± 2.8% after treatment with 1 μM. The result suggests that DOX treatment induces alterations in nuclear morphology which are characteristic of apoptosis. No apoptotic nuclei were observed for 6 h regardless of the concentration used (data not shown). The first significant results appeared for 12 h when 0.5 μM DOX was used (data not shown).

Doxorubicin effects on intracellular oxidative stress, mitochondrial membrane potential and cytosolic calcium

Early intracellular oxidative stress induced by DOX in H9c2 cells was detected by dichlorofluorescein (DCF) oxidation after exposure to 0.5 and 1 μM DOX for 6 h (Fig. 5a). Quantitation of mean DCF fluorescence intensity in control and treated cells was performed, showing a statistically significant increase in probe oxidation after both treatments (139.12 ± 12.64% for 0.5 μM DOX and 139.07 ± 7.91% for 1 μM DOX). The results confirmed that 0.5 and 1 μM DOX also cause increased oxidative stress in H9c2 myoblasts.

The DOX effects on mitochondrial transmembrane electric potential ($\Delta\psi$) were analyzed in DOX-treated cells by epifluorescence microscopy, by using TMRM as a $\Delta\psi$-selective probe. The results (Fig. 5b) were consistent with a decrease in mitochondrial $\Delta\psi$ in H9c2 cells after 6–24-h treatment with both 0.5 and 1 μM DOX. The results demonstrate once again that DOX treatment causes mitochondrial dysfunction even for a short incubation of 6 h. The results obtained by epifluorescent microscopy were confirmed by fluorimetric measurements, with cells in suspension pre-incubated with DOX and labeled with TMRM. The results obtained were similar (data not shown).

Alterations in cytosolic calcium induced by DOX in H9c2 cells were evaluated by epifluorescence microscopy using the ratiometric probe FURA-2/AM (Fig. 5c). When compared with untreated cells, an increase in intracellular calcium levels was observed after treatment with 0.5 and 1 μM DOX (146.98 ± 15.48% and 128.31 ± 11.2%, vs. control, respectively) for 6 h.

It is important to point out the alterations of oxidative stress, mitochondrial $\Delta\psi$ and calcium induced by DOX occurred before cell survival was compromised, as measured by LDH release (data not shown).

Pifithrin-alpha inhibition of cell death, caspases-9 and -3 activation and mitochondrial $\Delta\psi$ changes

To test the involvement of p53 in mitochondrial responses to DOX, cells were pre-incubated with the p53 inhibitor pifithrin-alpha prior to DOX treatment. Cell death, caspase-9 and -3 like activities and alterations in mitochondrial $\Delta\psi$ were selected as endpoints for measuring mitochondrial dysfunction. For these experiments, H9c2 cells were pre-incubated with 30 μM of pifithrin-alpha during 30 min before treating cells with 1 μM of DOX for 24 h (for cell death and caspase activities assays) or 6 and 12 h (for mitochondrial $\Delta\psi$ measurements).

The effect of pifithrin-alpha on DOX-induced H9c2 cell death was analyzed by SRB dye-binding assay (Fig. 6a). The data obtained demonstrate that 24-h treatment with

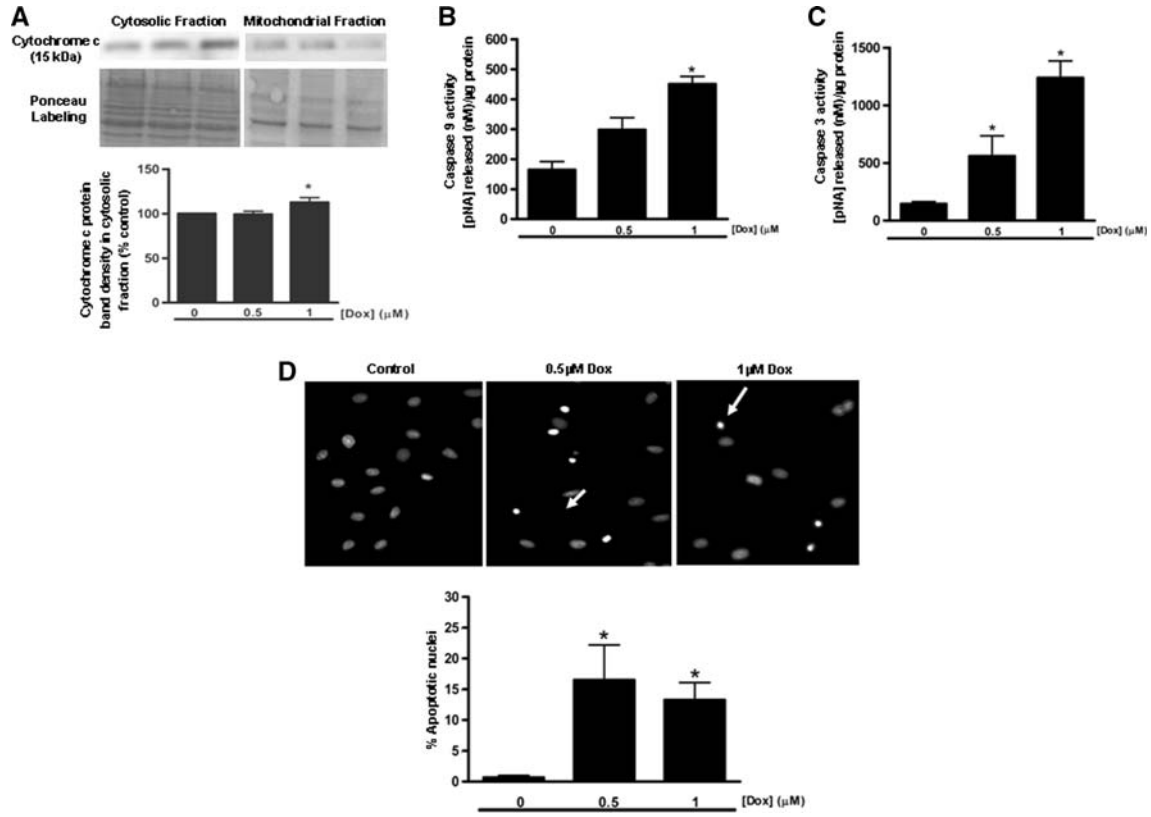

Fig. 4 Cytochrome *c* release from mitochondria, caspase 9 and caspase 3 activation and chromatin condensation after H9c2 cells treatment with DOX. **a** Western blot analysis of cytosolic and mitochondrial fractions collected from H9c2 cells after 24 h treatment with 0, 0.5 and 1 μM DOX. Cytosolic and mitochondrial fractions were collected as described in "Materials and methods" section. Western blot images are representative from five different experiments, producing similar results. *Ponceau labeling* shows the loading of equal amount of protein in each line. *Graph* represents the densitometric analysis of cytochrome *c* protein in cytosolic fractions, expressed as % of control. Data are expressed as mean ± SEM of five different experiments. Caspase-9 (**b**) and caspase-3 (**c**)-like activities were measured by following the cleavage of the colorimetric substrates Ac-LEHD-*p*NA and Ac-DEVD-*p*NA, respectively. The caspase-like activity was expressed as concentration of *p*NA released per μg protein. The results were calibrated with know concentrations of *p*-NA. Data are expressed as mean ± SEM of five different experiments. Statistical analysis $P < 0.05$ compared with control for the same time point. **d** Epifluorescence microscopy images of nuclei showing H9c2 cells treated with 0, 0.5 and 1 μM DOX during 24 h. Changes in nuclear morphology characteristic of apoptosis (*arrows*) were detected in Hoechst 33342-stained cells. *Scale bar* represents 40 μm. Apoptotic nuclei appear overexposed. *Graph* represents the numbers of apoptotic nuclei counted and expressed as the percentage of total cells counted (approximately 200 cells per coverslip). Data represents the mean ± SEM of five different experiments. Statistical analysis * $P < 0.05$ versus control for the same time point

1 μM DOX caused a decrease in cell numbers. Loss in cell numbers was significantly but not totally prevented by pifithrin-alpha, supporting the idea that the activation of p53 in H9c2 cells after DOX treatment can be, at least partially, responsible for its cytotoxic effect. Interestingly, the same protective effect was not observed after treatment with 0.5 μM DOX for 24 h.

Pifithrin-alpha effects on caspase-9 and -3 like activities were also evaluated (Fig. 6b). The data obtained show that the increase in caspase-9 and caspase-3 like activity caused by 1 μM DOX was totally prevented by pre-incubation of 30 μM pifithrin-alpha for 30 min. The results support the idea that p53 activity is required for caspase activation in H9c2 cells after treatment with 1 μM DOX.

Finally, we analyzed the effect of Pifithrin-alpha on mitochondrial $\Delta\psi$ (Fig. 6c). The results demonstrate that the decrease in mitochondrial $\Delta\psi$ observed after treatment with 1 μM of DOX was also prevented by pre-treatment with pifithrin-alpha. The results suggest that the increase in p53 quantity induced by 1 μM DOX treatment also occurs upstream of mitochondrial $\Delta\psi$ depolarization.

Effect of selected antioxidant molecules in H9c2 cell death induced by Doxorubicin

Oxidative stress has been reported as a prominent mechanism responsible for the cardiotoxicity associated with DOX therapy [3]. To test whether antioxidants can inhibit

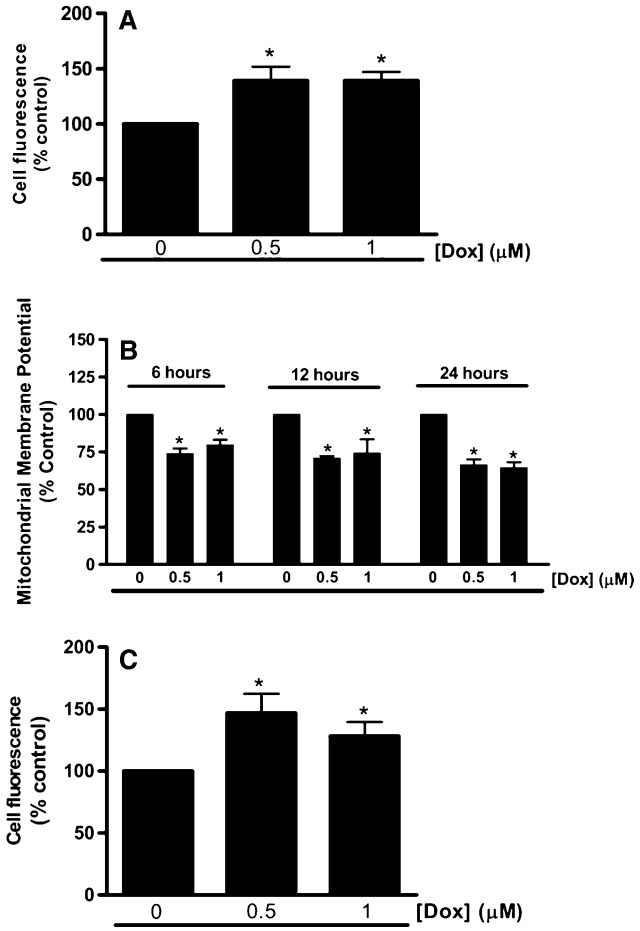

Fig. 5 Intracellular oxidative stress, mitochondrial depolarization and cytosolic calcium deregulation induced by DOX in H9c2 cells. **a** Early intracellular ROS production induced by DOX in H9c2 cells after 6 h treatment with 0, 0.5 and 1 μM. Increase in oxidative stress was detected by oxidation of dichlorofluorescein and observed by epifluorescence microscopy, as described in "Materials and methods" section. Results are expressed as percentage of control of mean DCF fluorescence intensity in each cell and represent the mean ± SEM of five different cell preparations. * $P < 0.05$ versus control. **b** Mitochondrial membrane potential of H9c2 cells treated with 0, 0.5 and 1 μM DOX for 6, 12 and 24 h. Mitochondrial membrane potential was determined by epifluorescence microscopy using the probe TMRM, as described in "Materials and methods" section. Results are expressed as percentage of control of mean cell fluorescence intensity and represent the mean ± SEM of four different cell preparations. * $P < 0.05$ versus control. **c** Cytosolic calcium levels detected in H9c2 cells after treatment with 0, 0.5 and 1 μM DOX for 6 h. Alterations in cytosolic calcium levels were detected by epifluorescence microscopy, using the probe Fura-2AM, as described in "Materials and methods" section. Results are expressed as percentage of control of mean cell fluorescence intensity and represent the mean ± SEM of eight different cell preparations. * $P < 0.05$ versus control

cell death induced by DOX, the effects of Trolox, vitamin E-succinate, and NAC were examined. The H9c2 cells were pre-incubated with 100 μM of trolox for 30 min, followed by treatment with 0.5 and 1 μM DOX for 24 h. Changes in H9c2 cell numbers due to DOX-induced cell

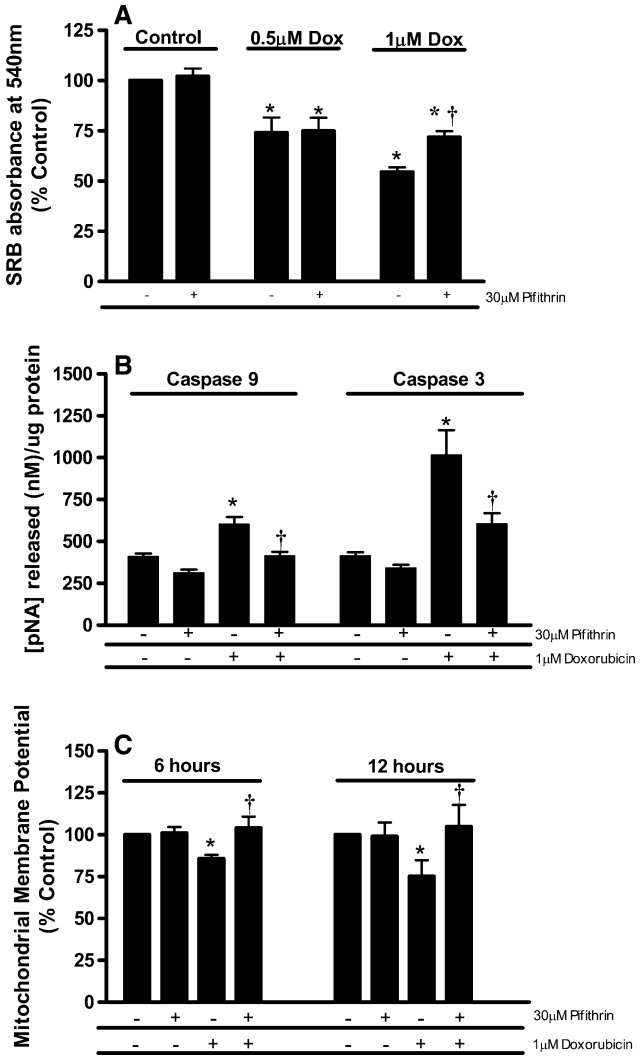

Fig. 6 Pifithrin-alpha effects on DOX-induced H9c2 cytotoxicity, increased caspase 9 and 3-like activity and mitochondrial depolarization. **a** Protective effect of pifithrin-alpha on DOX-induced cell death, analyzed by sulforhodamine B dye-binding assay. Cell treatment and analysis were performed as described in "Materials and methods" section. Data represent the mean ± SEM of six different cell preparations. **b** Effect of Pifithrin-alpha on DOX-mediated caspase 3 and 9-like activity. H9c2 cells pre-treated with 30 μM Pifithrin-alpha for 30 min were later incubated with 1 μM DOX for 24 h. Caspase 9 and caspase 3-like activities were measured by following the cleavage of colorimetric substrates Ac-LEHD-*p*NA and Ac-DEVD-*p*NA, respectively. The caspase-like activity was expressed as concentration of *p*NA released per μg protein. The results were calibrated with know concentrations of *p*-NA. Data are expressed as mean ± SEM of six separate experiments. **c** Effect of pifithrin-alpha on mitochondrial depolarization induced by DOX. After pre-incubation with 30 μM pifithrin-alpha for 30 min, H9c2 cells were treated with 1 μM DOX for 6 and 12 h. Mitochondrial membrane potential was later determined using the probe TMRM and visualized by epifluorescence microscopy as described in "Materials and methods" section. Results are expressed as percentage of control of mean cell fluorescence intensity and represents the mean ± SEM of six different cell preparations. Statistical analysis for all panels * $P < 0.05$ versus control (no DOX added); † $P < 0.05$ versus DOX treatment

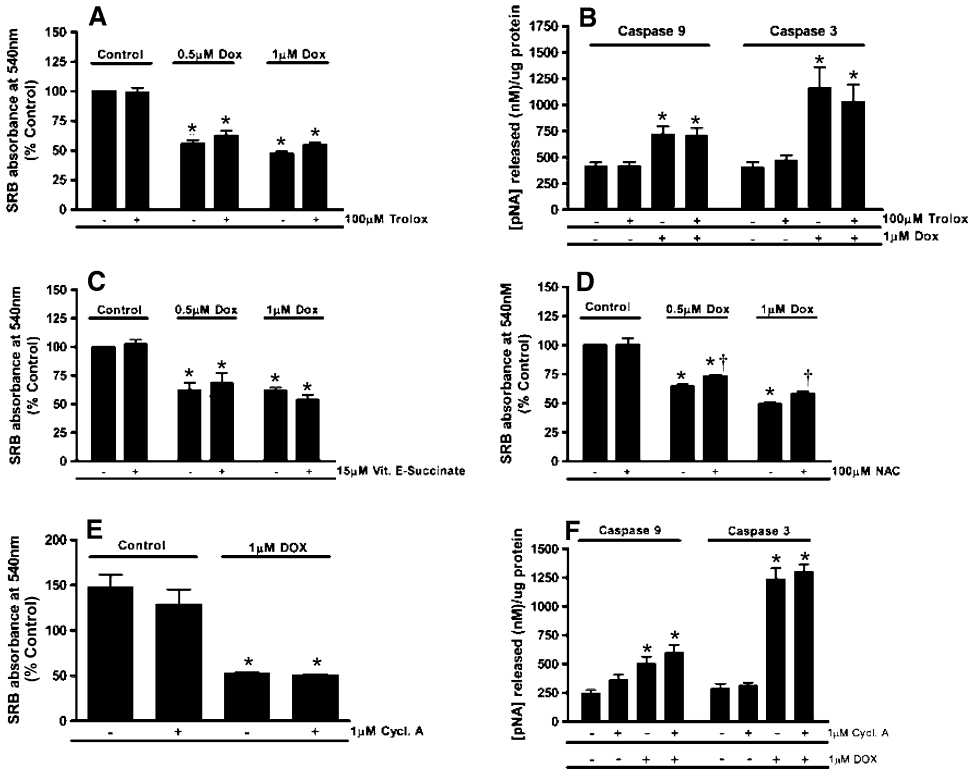

Fig. 7 Effect of antioxidants and the mitochondrial permeability transition pore inhibitor, cyclosporin-A, against DOX-induced cytotoxicity. The effect of Trolox on DOX-induced cell death in H9c2, analyzed by sulforhodamine B dye-binding assay (**a**) and by measurement of caspase-3 and caspase-9 like activities (**b**). After 30 min pre-incubation with 100 μM Trolox, H9c2 cells were treated with DOX for the described concentrations during 24 h. Results were analyzed as described in "Materials and methods" section. Data represent the mean ± SEM of six different cell preparations. **c** Effect of vitamin E-succinate on DOX-induced cytotoxicity. After pre-incubation with 15 μM vitamin E-succinate during 24 h, H9c2 cells were incubated with 0, 0.5 and 1 μM DOX for 24 h more and later analyzed by sulforhodamine B dye-binding assay. Data represent the mean ± SEM of six different cell preparations. **d** Effect of NAC on DOX-induced H9c2 cell loss. After a pre-incubation period of 2 h with 100 μM NAC, H9c2 cells were then treated with 0, 0.5 and 1 μM DOX for 24 h and results were analyzed by sulforhodamine B dye-binding assay. Data represent the mean ± SEM of four different cell preparations. **e** The effect of Cyclosporin A on DOX-induced H9c2 death, analyzed by sulforhodamine B dye-binding assay and **f** by measurement of caspase-3 and caspase-9 like activities. After 15 min pre-incubation with 1 μM Cyclosporin A, H9c2 cells were treated with DOX for the described concentrations during 24 h. Results were analyzed as described in "Materials and methods" section. The caspase-like activity was expressed as concentration of *p*NA released per μg protein. The results were calibrated with know concentrations of *p*-NA. Data are expressed as mean ± SEM of four to six different experiments. Statistical analysis for all panels * $P < 0.05$ versus control (no DOX added); † $P < 0.05$ versus respective DOX treatment

death were analyzed by SRB dye-binding assay (Fig. 7a). Caspase-9 and caspase-3 like activities (Fig. 7b) were also measured by following the cleavage of the colorimetric substrates Ac-LEHD-*p*NA and Ac-DEVD-*p*NA, respectively. The results demonstrate that Trolox did not prevent the decrease in cell numbers, the activation of caspase-9 and -3 (Fig. 7a, b) nor mitochondrial $\Delta\psi$ depolarization (data not shown). The effects of vitamin E-succinate and NAC were evaluated using SRB cell assays. The cells were pre-incubated with 15 μM of vitamin E-succinate for 24 h, followed by 0.5 and 1 μM DOX for 24 h. The results obtained demonstrated that vitamin E-succinate also did not prevent the reduction in cell numbers induced by DOX (Fig. 7c). The cells were also pre-incubated with 100 μM NAC for 2 h, followed by incubation with 0.5 and 1 μM DOX for 24 h. A marginal but significant effect on the reduction of cell death induced by DOX (8.8 ± 1.52% for 0.5 μM DOX and 9.1 ± 2.13% for 1 μM DOX) was observed (Fig. 7d). These results downplay the role of oxidative stress as a major cause of cardiac cell death caused by DOX.

Effects of cyclosporin A on DOX-induced caspases-3 and -9 activation and H9c2 cell death

The effect of cyclosporin A, a mitochondrial permeability transition (MPT) inhibitor [28], in cell death induced by DOX treatment was analyzed by using the SRB assay. Caspase-9 and -3 like activities were also evaluated by following the cleavage of the colorimetric substrates

Ac-LEHD-*p*NA and Ac-DEVD-*p*NA, respectively. The concentration of cyclosporin A used was based on preliminary experiments where the toxic threshold of cyclosporin A on H9c2 cells was evaluated (data not shown). After 15 min pre-incubation with 1 μM cyclosporin A, H9c2 myoblasts were incubated with 1 μM DOX for 24 h more. The results demonstrate that cyclosporin A did not prevent cell death or caspase-3 and -9 activation induced by DOX treatment in H9c2 myoblast cells (Fig. 7e, f).

Discussion

Several hypotheses have been proposed for the mechanism(s) of cardiotoxicity associated with DOX therapy. Free radical generation resulting in mitochondrial dysfunction and disruption of calcium homeostasis are the most common theories proposed to explain DOX cardiotoxicity [3, 29, 30]. However, recent studies have shown DNA damage as an early event in the toxicity induced by DOX in cardiac cells [15, 16, 22, 23]. Our initial work hypothesis was that mitochondrial dysfunction is a consequence of nuclear p53 activation, rather than a direct effect of the drug on mitochondria. We confirmed the hypothesis by identifying the protection afforded by pifithrin-alpha (a p53 inhibitor) against selected endpoints of mitochondrial dysfunction induced by DOX in H9c2 myoblasts. The conclusions were strengthened by the sequence of biochemical events verified after DOX cell treatment.

The present study demonstrates that DOX is primarily accumulated in the nucleus of H9c2 cells (Fig. 1a). Previous studies have shown that DOX interacts directly with DNA, via intercalation between adjacent base pairs of the double helical structure [31], or through induction of DNA interstrand cross-links. DOX–DNA binding has been shown to inhibit DNA interactions with transcription factors and RNA polymerase in cancer cells [13, 14]; similar effects may occur in cardiomyocytes. When DNA integrity is compromised in proliferating cells, DNA synthesis and consequently the cell cycle is interrupted while DNA is repaired [32]. The BrdU pulse labeling showed that DNA synthesis during cell proliferation was not markedly affected immediately after DOX addition, although a significant reduction in the numbers of cells synthesizing DNA was evident after 24 h of DOX treatment. The data suggest that DOX indirectly suppresses DNA synthesis in H9c2 cells by inducing cell cycle arrest. By comparing the time course of DOX nuclear uptake (Fig. 1b) with the inhibition of DNA synthesis (Fig. 1c), the result indicates that DOX enters the nucleus fairly rapidly (within 2–3 h), presumably damaging DNA and activating checkpoints that arrest cell cycle. One of the proteins involved in the cell responses to DNA damage is the transcription factor p53 [33]; p53 is involved in the activation of cell cycle checkpoints responsible for the arrest of cell cycle, DNA repair and apoptosis, once DNA stability is compromised [33]. The results shown in Fig. 2b reveal an increase in p53 quantity after 6 h of treatment with both 0.5 and 1 μM DOX, which was maintained for 12- and 24-h treatment. As p53 protein is activated during nuclear DNA damage, the results suggest that DOX damages nuclear DNA in H9c2 cells.

Bax was the first p53 regulated gene to be recognized as involved in the apoptotic process [34, 35]. In fact, 24 h after incubation with 0.5 and 1 μM DOX, a slight but significant increase in content of Bax protein was observed in H9c2 myoblasts (Fig. 2c). Furthermore, 24 h after DOX treatment, the formation of Bax clusters or foci was observed by immunocytochemistry of H9c2 cells (Fig. 3b). Confocal microscopy revealed that in several cells, Bax clusters were localized on or close to mitochondrial sites (Fig. 3c). The appearance of Bax aggregates was not so evident after treatment with 1 μM DOX for 24 h. We suppose that this result was due to an assay limitation, as dying cells (most likely with more numerous Bax clusters) were lost by detachment and thus could not be analyzed. The results resemble those reported by Brady et al. [36], where clustering of Bax was observed close to mitochondria in cardiac cells subjected to ischemia and reperfusion. Bax has been suggested to be translocated from the cytosol of cardiomyocytes in two distinct phases [37]. The first phase involves the formation of pores by the assembly of Bax oligomers in the outer mitochondrial membrane, promoting cytochrome *c* release [37, 38], and the second phase involves the sequestration of Bax from cytosol into large aggregates associated with mitochondria [37]. During the first phase, smaller Bax aggregates may also occur but are undetectable by fluorescent microscopy [37].

Western blotting confirmed the presence of Bax in mitochondria following DOX treatment (Fig. 3), although it is not possible to distinguish between Bax that was inserted into mitochondrial membranes (phase I) or Bax that was part of larger clusters that were associated with mitochondria (phase II) and also imaged by microscopy. The results also indicate that Bax translocation to mitochondria is a late event in the mechanism of DOX-induced toxicity.

A slight but significant increase of p53 was also present in mitochondrial fractions isolated from cells treated with 1 μM DOX for 24 h. In fact, previous studies have shown that p53 protein can behave as a pro-apoptotic factor when directly translocated to mitochondria [21]. The appearance of cytochrome *c* in cytosolic fractions of H9c2 cells treated with 1 μM DOX for 24 h (Fig. 4a) was also observed by Western blot. Downstream events, such as caspase-9 (Fig. 4b) and caspase-3-like (Fig. 4c) activities were also evaluated. The results support the hypothesis that 1 μM

DOX treatment for 24 h induces cytochrome *c* release from mitochondria, promoting the activation of caspases. After treatment with 0.5 μM DOX, a statistically significant activity was only observed for caspase-3. Moreover, it is also important to note that after 24-h treatment with 0.5 μM DOX, no statistically significant appearance of cytochrome *c* in cytosolic fraction was observed. These results suggest that in H9c2 cells, 0.5 μM DOX was not enough to activate mitochondrial-dependent apoptotic pathway but could activate caspase-3 and promote apoptosis through mechanisms other than the classic mitochondrial-dependent pathway. In fact, there is evidence that DOX can also induce apoptosis in cardiac cells through the Fas-mediated pathway [39]. One end-result of DOX-induced apoptosis was chromatin condensation, observed in H9c2 cells when exposed to 0.5 and 1 μM DOX for 24 h (Fig. 4d).

Oxidative stress and consequent mitochondrial dysfunction and cytosolic calcium deregulation are consequences of the direct effects of DOX on cardiac mitochondria [3, 29]. We observed that H9c2 cells, after treatment with 0.5 and 1 μM DOX, presented the same type of events as soon as 6 h after drug addition (Fig. 5a–c). As has been shown for cardiac myocytes, it is possible that DOX accumulates in the mitochondria of H9c2 cells and undergoes redox cycling on complex I of the respiratory chain, thereby increasing oxidative stress with consequent loss of mitochondrial membrane potential and ability to modulate cytosolic calcium levels [29].

In order to investigate the relevance of two different mechanisms of DOX toxicity (nuclear p53 activation vs. oxidative stress) for H9c2 cell death, pifithrin-alpha (p53 inhibitor) and selected antioxidants (trolox, vitamin-E succinate and NAC) were used. The results from this study indicate that p53 activation is an important event in DOX-induced H9c2 cell death. In fact, Liu et al. [17] proposed pifithrin-alpha as a potential preventive agent for cardiac toxicity induced by DOX therapy. The results presented herein demonstrated that pifithrin-alpha can protect H9c2 cells from mitochondrial membrane potential disruption (Fig. 6c) and caspase-9 and caspase-3 activation (Fig. 6b), which were chosen as end-points for mitochondrial dysfunction. However, in spite of attenuated cell death (Fig. 6a), total protection was not observed. Furthermore, pifithrin-alpha did not prevent H9c2 cell death upon treatment with 0.5 μM DOX for 24 h (Fig. 6a). The observation suggests that DOX treatment (especially at lower concentrations), may also activate other mechanisms that induce H9c2 cell death in a p53-independent way. This possibility remains to be explored.

Despite the well-documented role of oxidative stress on the pathogenesis of DOX cardiotoxicity, not all antioxidants are effective cytoprotectives [40, 41]. Three different antioxidant compounds (trolox, vitamin E-succinate and NAC) were evaluated for their protective effect on H9c2 cell death induced by DOX treatment for 24 h. Trolox is a water-soluble analog of vitamin E lacking the phytyl chain and exhibiting high antioxidant activity [42]. Vitamin E-succinate is an esterified form of vitamin E, less hydrophobic and more readily taken up by cells rapidly enriching cellular membranes, including mitochondria, with protective levels of vitamin E [43]. In spite of having powerful antioxidant activity in the H9c2 cell line against other pro-oxidants [44], trolox and vitamin E-succinate did not prevent the cell loss induced by DOX treatment in the present study (Fig. 7a–c). Regarding vitamin E-succinate, we observed that higher concentrations of the compound caused cell death by itself. We also should be aware that the lack of protection by some antioxidants may be due to a limited partition of the antioxidants to critical cellular sites. When H9c2 myoblasts were pre-incubated with NAC for 2 h before DOX treatment, a partial prevention in the decrease of cell mass upon DOX treatment (Fig. 7d) was observed. NAC is the acetylated form of the amino acid L-cysteine and a source of sulfhydryl (SH) groups. In the body, NAC is converted to metabolites capable of stimulating glutathione (GSH) synthesis and can also directly act as free radical scavenger [45, 46]. Interestingly, higher protection with NAC was observed when oxidative stress in H9c2 myoblasts was induced by the pro-oxidant compound tert-butyl hydroperoxide [44]. Our data suggest that in spite of being considered a major cause for the loss of cardiomyocytes after DOX treatment, oxidative stress is not the only factor responsible for DOX-induced cell death. In fact, it has been previously demonstrated that a diet rich in vitamin E-succinate failed to protect against mitochondrial dysfunction and cardiac histopathology associated with DOX treatment [40]. The authors suggested that oxidative stress by itself is not the only factor responsible for the persistent mitochondrial cardiomyopathy associated with long-term DOX therapy [40]. However, oxidative stress may have other important roles on the pathogenesis of DOX toxicity. In fact, it has been proposed that during treatment with some anti-neoplastic agents, enhanced generation of ROS mediates the formation of disulfide bridges between cytosolic Bax monomers, which results in formation of mitochondrial outer membrane channels [47].

Opening of the MPT pore has been described as an event occurring in mitochondria during oxidative stress and calcium deregulation [48]. Interestingly, enhanced induction of MPT pore was also observed in mitochondria isolated from hearts of DOX-treated rats, the reduced calcium loading capacity derived from MPT pore being considered a sensitive and reliable marker of DOX cardiotoxicity [49, 50]. Cyclosporin A, a MPT pore inhibitor [28], was able to prevent the enhanced induction of the MPT pore in mitochondria harvested from hearts of DOX-treated rats [50].

However, in H9c2 myoblasts, cyclosporin A did not prevent cell death or caspase-9 and -3 activation (Fig. 7e, f). The result suggests that the MPT pore is not a primary cause of H9c2 myoblast death and that mechanistical differences exist between cyclosporin A effects on intact cells versus isolated cardiac mitochondria.

According to the results presented in this study, an increase in ROS production, cytosolic calcium deregulation, mitochondrial depolarization and an increase in p53 quantity were all early markers for DOX cytotoxicity on H9c2 myoblast, occurring as early as 6 h after treatment. On the other hand, caspase activation, chromatin condensation and ultimately cell death are late events. Translocation of p53 and Bax to mitochondria followed by the formation of Bax clusters and cytochrome *c* release were observed in H9c2 after 24-h treatment with DOX. Although several intermediate time points were not explored, it is possible to propose an integrated model for the effect of DOX in H9c2 myoblast cells (Fig. 8). According to the model, DOX is incorporated in the nucleus and interferes with DNA replication and transcription. Consequently, p53 is activated and translocated to mitochondrial membranes, although the exact events that occur downstream to such process are still not understood. Once activated, p53 can also act as a transcription factor, promoting an increase in the expression of pro-apoptotic proteins, such as Bax, which can also be translocated to mitochondrial membranes and interfere with mitochondrial function. A consequence of Bax translocation to mitochondrial membranes is the formation of Bax clusters which were for the first time imaged on DOX-treated cardiac cells.

It has been previously published that the loss of cardiac cells by apoptosis is a relevant process during myocardial dysfunction [51–53]. In fact, DOX-induced apoptosis has also been considered one major cause of DOX-induced cardiotoxicity [54]. Results observed in in vivo and in vitro models confirm the relevance of apoptosis during DOX-induced cardiotoxicity, although the magnitude of the phenomenon among cells varies with the model [11, 12, 55]. Our studies were performed in H9c2 myoblasts, which are an accepted cellular model for cardiac cells, being also widely used to study DOX-induced cardiotoxicity. It appears clear that in order to support our conclusions and to identify differences in the apoptotic response resulting from the model used, further studies using isolated cardiac myocytes and/or animal models need to be performed. Despite this apparent drawback, we think that although the percentage of apoptosis detected in vivo or in isolated adult cardiac myocytes may be different from the percentage of apoptosis observed in the present study, the pathways activated by DOX treatment may be very similar.

In conclusion, the present work demonstrates that (a) mitochondrial dysfunction in DOX-treated H9c2 myoblasts is secondary to p53 activation (b) cytosolic Bax clusters occur after DOX treatment on H9c2 myoblasts, (c) despite previously published work demonstrating oxidative stress as a major player on DOX-induced cardiotoxicity, selected antioxidant molecules were of limited effect against DOX-induced H9c2 cell death and (d) MPT pore opening does not appear to be the primary cause of H9c2 cell death induced by DOX treatment.

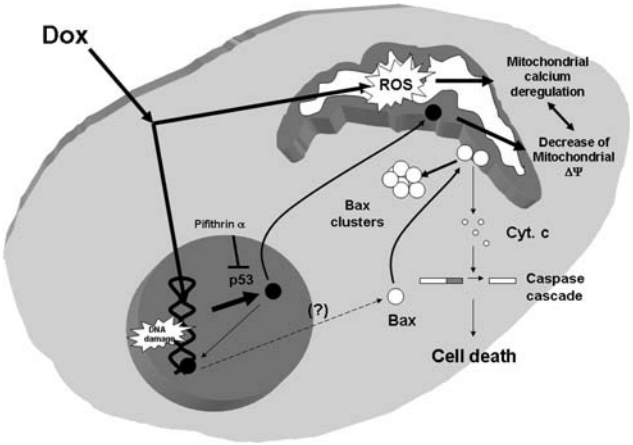

Fig. 8 A model showing the proposed mechanism by which DOX induces H9c2 cell death. After treatment, DOX is accumulated in the nucleus and interferes with DNA physiology, which may involve increased damage. Due to DNA damage, p53 is overexpressed and activated. Working as a pro-apoptotic factor, p53 is translocated to mitochondrial membrane, promoting mitochondrial dysfunction and release of apoptogenic factors retained between the inner and outer mitochondrial membranes (such as cytochrome *c*), activating the mitochondrial dependent apoptotic pathway. Furthermore, once activated, p53 can also act as a transcription factor, promoting an increase in the expression of pro-apoptotic proteins such as Bax. Bax can also be translocated to mitochondrial membranes, interfering with mitochondrial integrity and inducing cell death. On the other side, DOX can also suffer redox cycle in mitochondria, increasing oxidative stress, mitochondrial dysfunction and contributing to cytosolic calcium deregulation. It is proposed that Bax and p53 are intermediaries between nuclear and mitochondrial-based apoptotic pathways

Acknowledgments This work was supported by NIH grant HL 58016 and FCT SAU-OSM-64084-2006. Vilma A. Sardão is supported by grants from the Portuguese Foundation for Science and Technology, SFRH/BD/10251/2002 and SFRH/BPD/31549/2006. We acknowledge Ana Filipa Branco for excellent technical assistance. We also acknowledge Dr. Marc Fariss (University of Colorado, Denver) for providing vitamin E-succinate.

Conflict of interest statement None.

References

1. Doroshow JH, Davies KJ (1986) Redox cycling of anthracyclines by cardiac mitochondria. II. Formation of superoxide anion, hydrogen peroxide, and hydroxyl radical. J Biol Chem 261:3068–3074

2. Davies KJ, Doroshow JH (1986) Redox cycling of anthracyclines by cardiac mitochondria. I. Anthracycline radical formation by NADH dehydrogenase. J Biol Chem 261:3060–3067
3. Wallace KB (2003) Doxorubicin-induced cardiac mitochondrionopathy. Pharmacol Toxicol 93:105–115
4. Goormaghtigh E, Pollakis G, Ruysschaert JM (1983) Mitochondrial membrane modifications induced by adriamycin-mediated electron transport. Biochem Pharmacol 32:889–893
5. Mimnaugh EG, Trush MA, Gram TE (1983) Enhancement of rat heart microsomal lipid peroxidation following doxorubicin treatment in vivo. Cancer Treat Rep 67:731–733
6. Palmeira CM, Serrano J, Kuehl DW et al (1997) Preferential oxidation of cardiac mitochondrial DNA following acute intoxication with doxorubicin. Biochim Biophys Acta 1321:101–106
7. Solem LE, Wallace KB (1993) Selective activation of the sodium-independent, cyclosporin A-sensitive calcium pore of cardiac mitochondria by doxorubicin. Toxicol Appl Pharmacol 121:50–57
8. Bernardi P (1996) The permeability transition pore. Control points of a cyclosporin A-sensitive mitochondrial channel involved in cell death. Biochim Biophys Acta 1275:5–9
9. Crompton M (1999) The mitochondrial permeability transition pore and its role in cell death. Biochem J 341(Pt 2):233–249
10. Di Lisa F (2001) Mitochondrial contribution in the progression of cardiac ischemic injury. IUBMB Life 52:255–261
11. Childs AC, Phaneuf SL, Dirks AJ et al (2002) Doxorubicin treatment in vivo causes cytochrome *c* release and cardiomyocyte apoptosis, as well as increased mitochondrial efficiency, superoxide dismutase activity, and Bcl-2:Bax ratio. Cancer Res 62:4592–4598
12. Yamanaka S, Tatsumi T, Shiraishi J et al (2003) Amlodipine inhibits doxorubicin-induced apoptosis in neonatal rat cardiac myocytes. J Am Coll Cardiol 41:870–878
13. Cutts SM, Nudelman A, Rephaeli A et al (2005) The power and potential of doxorubicin-DNA adducts. IUBMB Life 57:73–81
14. Cutts SM, Parsons PG, Sturm RA et al (1996) Adriamycin-induced DNA adducts inhibit the DNA interactions of transcription factors and RNA polymerase. J Biol Chem 271:5422–5429
15. L'Ecuyer T, Sanjeev S, Thomas R et al (2006) DNA damage is an early event in doxorubicin-induced cardiac myocyte death. Am J Physiol Heart Circ Physiol 291:H1273–H1280
16. Chua CC, Liu X, Gao J et al (2006) Multiple actions of pifithrin-alpha on doxorubicin-induced apoptosis in rat myoblastic H9c2 cells. Am J Physiol Heart Circ Physiol 290:H2606–H2613
17. Liu X, Chua CC, Gao J et al (2004) Pifithrin-alpha protects against doxorubicin-induced apoptosis and acute cardiotoxicity in mice. Am J Physiol Heart Circ Physiol 286:H933–H939
18. Shizukuda Y, Matoba S, Mian OY et al (2005) Targeted disruption of p53 attenuates doxorubicin-induced cardiac toxicity in mice. Mol Cell Biochem 273:25–32
19. Marchenko ND, Zaika A, Moll UM (2000) Death signal-induced localization of p53 protein to mitochondria. A potential role in apoptotic signaling. J Biol Chem 275:16202–16212
20. Moll UM, Zaika A (2001) Nuclear and mitochondrial apoptotic pathways of p53. FEBS Lett 493:65–69
21. Schuler M, Green DR (2001) Mechanisms of p53-dependent apoptosis. Biochem Soc Trans 29:684–688
22. Nithipongvanitch R, Ittarat W, Cole MP et al (2007) Mitochondrial and nuclear p53 localization in cardiomyocytes: redox modulation by doxorubicin (Adriamycin)? Antioxid Redox Signal 9:1001–1008
23. Nithipongvanitch R, Ittarat W, Velez JM et al (2007) Evidence for p53 as guardian of the cardiomyocyte mitochondrial genome following acute adriamycin treatment. J Histochem Cytochem 55:629–639
24. Kimes BW, Brandt BL (1976) Properties of a clonal muscle cell line from rat heart. Exp Cell Res 98:367–381
25. L'Ecuyer T, Horenstein MS, Thomas R et al (2001) Anthracycline-induced cardiac injury using a cardiac cell line: potential for gene therapy studies. Mol Genet Metab 74:370–379
26. Frost BM, Eksborg S, Bjork O et al (2002) Pharmacokinetics of doxorubicin in children with acute lymphoblastic leukemia: multi-institutional collaborative study. Med Pediatr Oncol 38:329–337
27. Klein D, Kern RM, Sokol RZ (1995) A method for quantification and correction of proteins after transfer to immobilization membranes. Biochem Mol Biol Int 36:59–66
28. Broekemeier KM, Dempsey ME, Pfeiffer DR (1989) Cyclosporin A is a potent inhibitor of the inner membrane permeability transition in liver mitochondria. J Biol Chem 264:7826–7830
29. Berthiaume JM, Wallace KB (2007) Adriamycin-induced oxidative mitochondrial cardiotoxicity. Cell Biol Toxicol 23:15–25
30. Hamza A, Amin A, Daoud S (2008) The protective effect of a purified extract of Withania somnifera against doxorubicin-induced cardiac toxicity in rats. Cell Biol Toxicol 24:63–73
31. Box VG (2007) The intercalation of DNA double helices with doxorubicin and nagalomycin. J Mol Graph Model 26:14–19
32. Kaufmann WK, Paules RS (1996) DNA damage and cell cycle checkpoints. FASEB J 10:238–247
33. Gomez-Lazaro M, Fernandez-Gomez FJ, Jordan J (2004) p53: twenty-five years understanding the mechanism of genome protection. J Physiol Biochem 60:287–307
34. Miyashita T, Krajewski S, Krajewska M et al (1994) Tumor suppressor p53 is a regulator of bcl-2 and bax gene expression in vitro and in vivo. Oncogene 9:1799–1805
35. Miyashita T, Reed JC (1995) Tumor suppressor p53 is a direct transcriptional activator of the human bax gene. Cell 80:293–299
36. Brady NR, Hamacher-Brady A, Gottlieb RA (2006) Proapoptotic BCL-2 family members and mitochondrial dysfunction during ischemia/reperfusion injury, a study employing cardiac HL-1 cells and GFP biosensors. Biochim Biophys Acta 1757:667–678
37. Capano M, Crompton M (2002) Biphasic translocation of Bax to mitochondria. Biochem J 367:169–178
38. Suzuki M, Youle RJ, Tjandra N (2000) Structure of Bax: coregulation of dimer formation and intracellular localization. Cell 103:645–654
39. Nakamura T, Ueda Y, Juan Y et al (2000) Fas-mediated apoptosis in adriamycin-induced cardiomyopathy in rats: in vivo study. Circulation 102:572–578
40. Berthiaume JM, Oliveira PJ, Fariss MW et al (2005) Dietary vitamin E decreases doxorubicin-induced oxidative stress without preventing mitochondrial dysfunction. Cardiovasc Toxicol 5:257–267
41. Wattanapitayakul SK, Chularojmontri L, Herunsalee A et al (2005) Screening of antioxidants from medicinal plants for cardioprotective effect against doxorubicin toxicity. Basic Clin Pharmacol Toxicol 96:80–87
42. Albertini R, Abuja PM (1999) Prooxidant and antioxidant properties of Trolox C, analogue of vitamin E, in oxidation of low-density lipoprotein. Free Radic Res 30:181–188
43. Fariss MW, Zhang JG (2003) Vitamin E therapy in Parkinson's disease. Toxicology 189:129–146
44. Sardão VA, Oliveira PJ, Holy J et al (2007) Vital imaging of H9c2 myoblasts exposed to tert-butylhydroperoxide—characterization of morphological features of cell death. BMC Cell Biol 8:11
45. Flora SJ (2007) Role of free radicals and antioxidants in health and disease. Cell Mol Biol 53:1–2
46. Kelly GS (1998) Clinical applications of *N*-acetylcysteine. Altern Med Rev 3:114–127
47. Neuzil J, Wang XF, Dong LF et al (2006) Molecular mechanism of 'mitocan'-induced apoptosis in cancer cells epitomizes the multiple roles of reactive oxygen species and Bcl-2 family proteins. FEBS Lett 580:5125–5129
48. Halestrap AP (2006) Calcium, mitochondria and reperfusion injury: a pore way to die. Biochem Soc Trans 34:232–237

49. Zhou S, Starkov A, Froberg MK et al (2001) Cumulative and irreversible cardiac mitochondrial dysfunction induced by doxorubicin. Cancer Res 61:771–777
50. Oliveira PJ, Bjork JA, Santos MS et al (2004) Carvedilol-mediated antioxidant protection against doxorubicin-induced cardiac mitochondrial toxicity. Toxicol Appl Pharmacol 200:159–168
51. Narula J, Haider N, Virmani R et al (1996) Apoptosis in myocytes in end-stage heart failure. N Engl J Med 335:1182–1189
52. Kang PM, Izumo S (2003) Apoptosis in heart: basic mechanisms and implications in cardiovascular diseases. Trends Mol Med 9:177–182
53. Haunstetter A, Izumo S (1998) Apoptosis: basic mechanisms and implications for cardiovascular disease. Circ Res 82:1111–1129
54. Kalyanaraman B, Joseph J, Kalivendi S et al (2002) Doxorubicin-induced apoptosis: implications in cardiotoxicity. Mol Cell Biochem 234–235:119–124
55. Youn HJ, Kim HS, Jeon MH et al (2005) Induction of caspase-independent apoptosis in H9c2 cardiomyocytes by adriamycin treatment. Mol Cell Biochem 270:13–19